Two-Dimensional Conductive Mesopore Engineering of Ultrahigh Content Covalent Sulfur-Doped Carbon for Superior Sodium Storage

Jie He,[a, b] Zhihao Sun,[c] Lei Huang,[a] Zijia Zhu,[b] Wei Luo,[c]* Dongliang Chao,[b]* Fanxing Bu[b]*

[a] State Key Laboratory for Modification of Chemical Fibers and Polymer Materials, College of Materials Science and Engineering, Donghua University, Shanghai 201620, P. R. China.

[b] Key Laboratory of Silicate Cultural Relics Conservation, School of Cultural Heritage and Information Management, Shanghai University, Shanghai 200444, China

[c] Department of Chemistry, Laboratory of Advanced Materials, State Key Laboratory of Molecular Engineering of Polymers, and Collaborative Innovation Center of Chemistry for Energy Materials, Fudan University, Shanghai 200433, P.R. China

Email: wluo@dhu.edu.cn

chaod@fudan.edu.cn

fxbu@shu.edu.cn

Experimental Section

Synthesis of Ti_3C_2: Ti_3C_2 was prepared by modified minimally intensive layer delamination (MILD) method developed by our group.[1] Briefly, 8.0 g of LiF was added to 100 mL of 9 M HCl at room temperature, and the mixture was stirred for 10 min to form the etchant. Then 5.0 g of Ti_3AlC_2 was slowly added into the above solution within 10 min to alleviate the initial overheating reaction. Successively, the reaction system was transferred to a 35 °C oil bath and then stirred for 24 h. The etched Ti_3C_2 was washed with large amount of water to remove acid, metal ions and LiF. When the pH value of the supernatant reached 7, the obtained Ti_3C_2 precipitation was added into 30 mL of DMSO and stirred for 12 h to increase their interlayer spacing. Later, the resulting colloidal solution was centrifuged and then washed with water twice. Subsequently, the expanded Ti_3C_2 was added into 200 mL of water and sonicated for 30 min under Ar protection. And then, the obtained colloidal dispersion was subjected to 40 min of centrifugation at 3500 rpm to remove any aggregates. Finally, the obtained few-layer Ti_3C_2 solution was collected and stored at 4 °C for the following experiments.

Preparation of highly ordered MesoPDA@Ti_3C_2: The highly ordered MesoUSC@Ti_3C_2 was prepared by one inorganic salt-mediated interfacial self-assembly route. Typically, 1 mL of 10 mg/mL Ti_3C_2 was added into 9 mL of deionized water under stirring for 10 min to form uniform dispersion. And then 10 mL of 20 mg/mL F127 ethanol solution, 2.0 mL of TMB, 100 mg of dopamine and 1 mmol of KCl were added into above solution one by one with 10 min interval. Subsequently, 0.5 mL of ammonia solution was added to induce the polymerization of dopamine and the reaction was allowed to run for 12 h. The products were collected by centrifugation and washed with water and ethanol three times, respectively. The MesoPDA@Ti_3C_2 with low order degree was fabricated in the same way without the adding of KCl, the MesoPDA was fabricated in the same way without the adding of Ti_3C_2 and KCl.

Preparation of highly ordered MesoUSC@Ti_3C_2: The highly ordered MesoUSC@Ti_3C_2 was obtained by one-step sulfidation treatment of MesoPDA@Ti_3C_2. Typically, MesoPDA@Ti_3C_2 and sulfur powder with mass ratio of

1:10 were put into ceramic crucial, and the heating temperature was increased to 600 °C at a rate of 5 °C/min, and maintained for 2 h under nitrogen atmosphere. The MesoUSC was fabricated in the same way by using its corresponding precursor.

Material Characterizations: The morphology and microstructure characterizations were conducted on Zeiss Ultra-55 field emission scanning eletron microscope (FESEM) and FEI Tecnai G2 20TWIN Transmission electron microscope (TEM, 200 kV). Nitrogen sorption isotherms were measured at 77 K with a Micromeritics Tristar 3020 analyzer. The specific surface area and the pore size distribution were calculated by using the Brunauer-Emmett-Teller (BET) and Barrett-Joyner-Halenda (BJH) method, respectively. The pore size distribution was calculated from the adsorption branch of isotherm. Small-angle X-ray Scattering (SAXS) measurements were carried out on Xeuss 2.0 using Cu KR radiation (40 kV, 35 mA). X-ray diffraction (XRD) analysis from 10° to 80° was carried out on PANalytical X' pert PRO X-ray diffraction (Cu Kα). X-ray photoelectron spectroscopy (XPS) was conducted on PHI 5000C ESCA system. Raman spectra were tested on XploRA Laser Raman Spectrometer. The time-of-flight secondary ion mass spectroscopy (ToF-SIMS) were obtained from a commercial ION-TOF GmbH mass spectrometer with a Bi^{3+} ion gun (30 keV). Pyris1 Thermo gravimetric analysis (TGA) was used to fulfill TGA test at a heating rate of 10 °C/min under nitrogen and air condition from 50-900 °C.

Electrochemical Characterizations: For the fabrication of working electrode, the highly ordered MesoUSC@Ti_3C_2, carbon nanotubes and polyvinylidene fluoride (PVDF) binder were mixed in a mass ratio of 7: 2: 1 to form a homogeneous slurry. The slurry was spread onto copper foil and vacuum dried at 100 °C for 12 h. The dried foil sheet was directly cut into circular disk as anode. Sodium ion battery was assembled in an argon-filled glove box with metallic sodium and glass fiber as counter electrode and separator, respectively. 1 M $NaPF_6$ in diglyme was used as the electrolyte. 2016 coin-type cell was employed for coin-cell battery. The galvanostatic experiments were carried out on a battery testing system (LAND, Wuhan China) in the voltage window from 0.01 V to 3 V at different current densities. Electrochemical impedance

spectroscopy (EIS) was tested on CHI 760D electrochemical workstation in the frequency range of 100 kHz to 0.01 Hz. Cyclic voltammetry (CV) curves at different scanning rate from 0.2 mV/s to 2 mV/s were also recorded at CHI 760D electrochemical workstation in the potential range of 0.01-3 V.

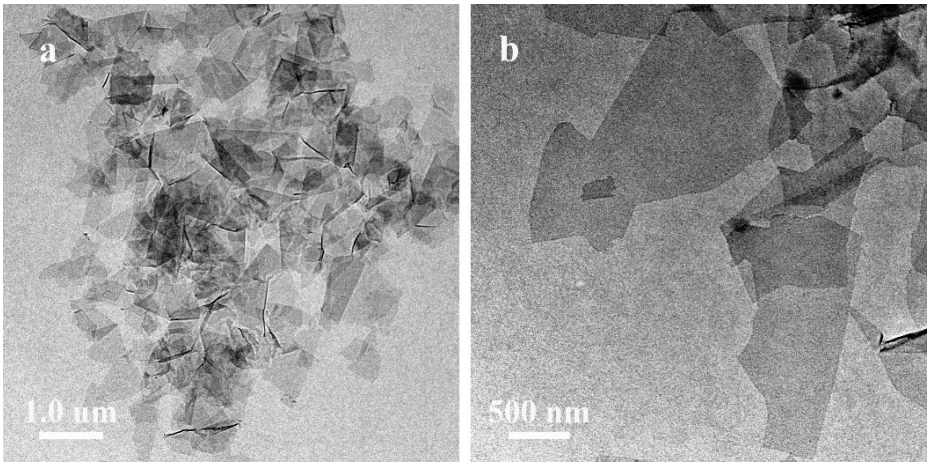

Figure S1. TEM images of Ti_3C_2 nanosheets

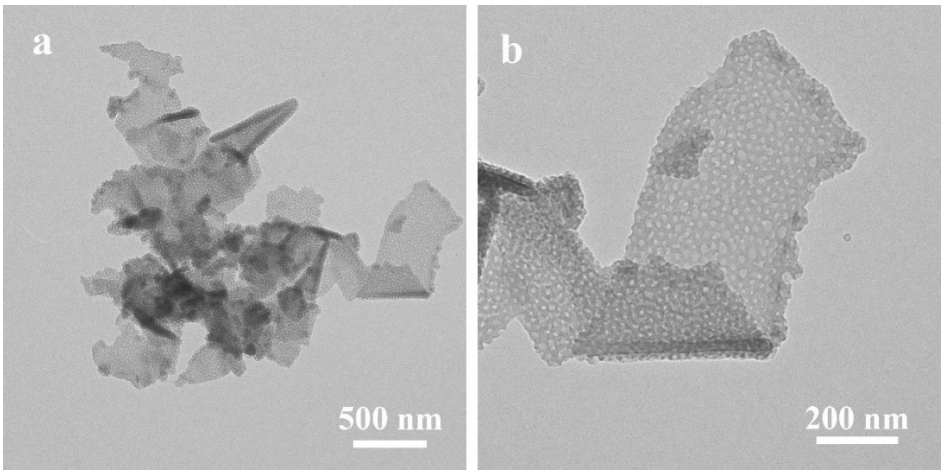

Figure S2. TEM images of MesoPDA@Ti_3C_2 prepared in the absence of KCl.

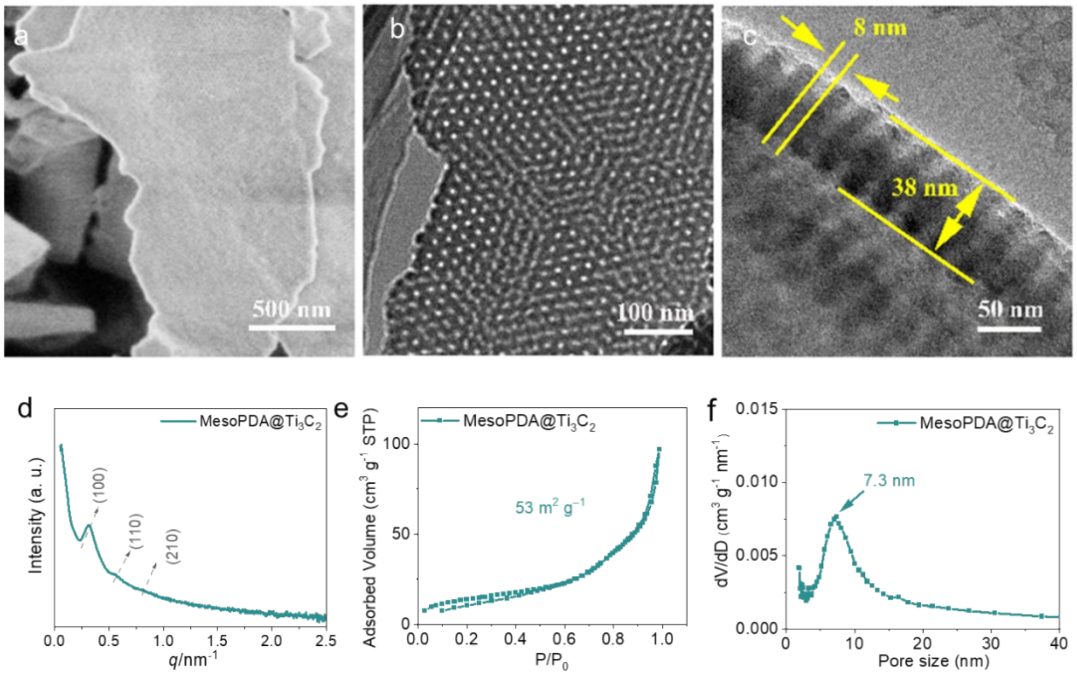

Figure S3. (a) SEM and (b, c) TEM, (d) SAXS, (e) N_2 sorption isotherms and (f) pore size distribution curves of the highly ordered MesoPDA@Ti_3C_2.

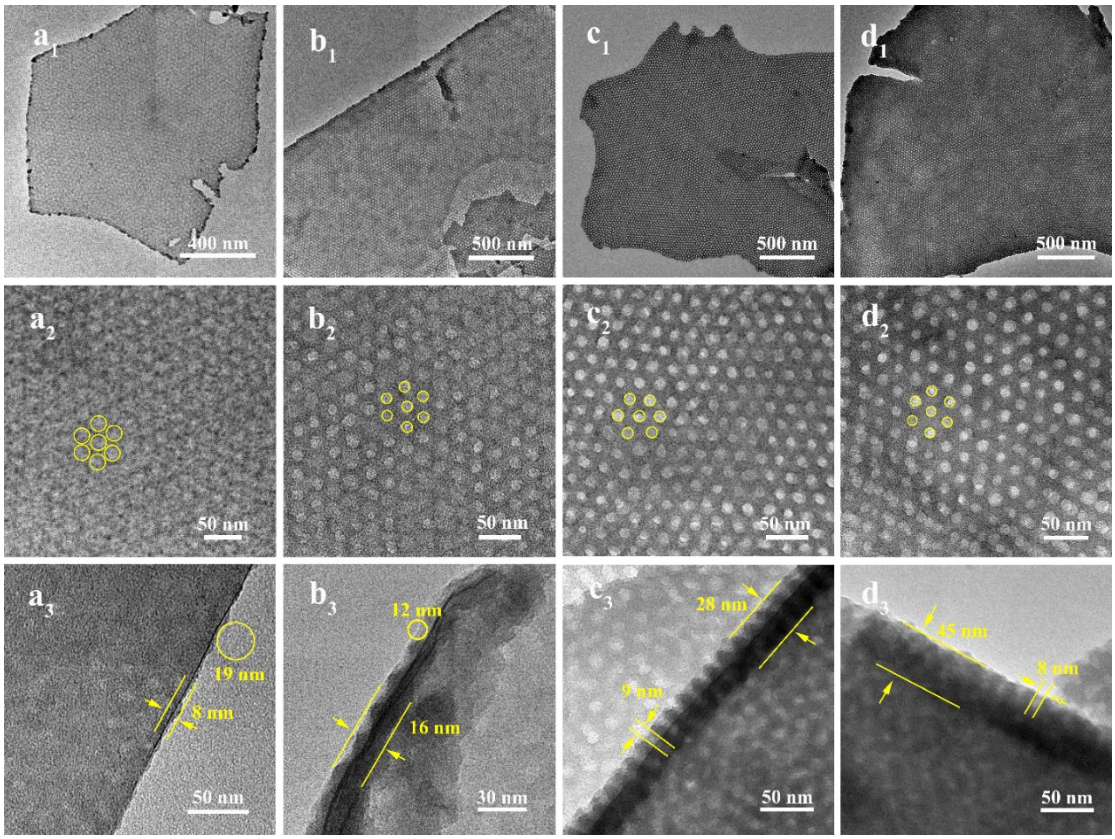

Figure S4. TEM images of highly ordered MesoPDA@Ti_3C_2 obtained at different reaction time. (a) 1 h, (b) 2 h, (c) 8 h, (d) 16 h.

The time-dependent experiments were carried out to gain insight for the self-assembly of the TMB/F127/PDA composited micelles to MesoPDA@Ti_3C_2. After stirring for 1 h, shallow pits with highly ordered arrangement have formed on Ti_3C_2 MXene nanosheet (Figure S3a_1-a_3). Cross-section TEM picture demonstrates that the thickness of mesoporous PDA is about 8 nm, and those pits possess spherical crown-like morphology. When prolonging the reaction time to 2 h, highly ordered mesoporous PDA with bowl-like structure appears on Ti_3C_2 MXene nanosheet, and the thickness of mesoporous PDA increases to 16 nm (Figure S3b_1-b_3). Further reaction time creates mesoporous PDA with vertical mesopores (Figure S3c_1-c_3, 3d_1-d_3), and the depth of them can gradually increase from 14 nm (8 h) to 19 nm (12 h) and then 22.5 nm (16 h). To be noted, the pore size decreases while the pore wall thickness increases along with the growth of mesoporous PDA at the initial stage (before 8 h). It is possible that part of TMB spilled out from the PPO section, and extra PDA oligomers diffused to those sections and polymerized to fill them.

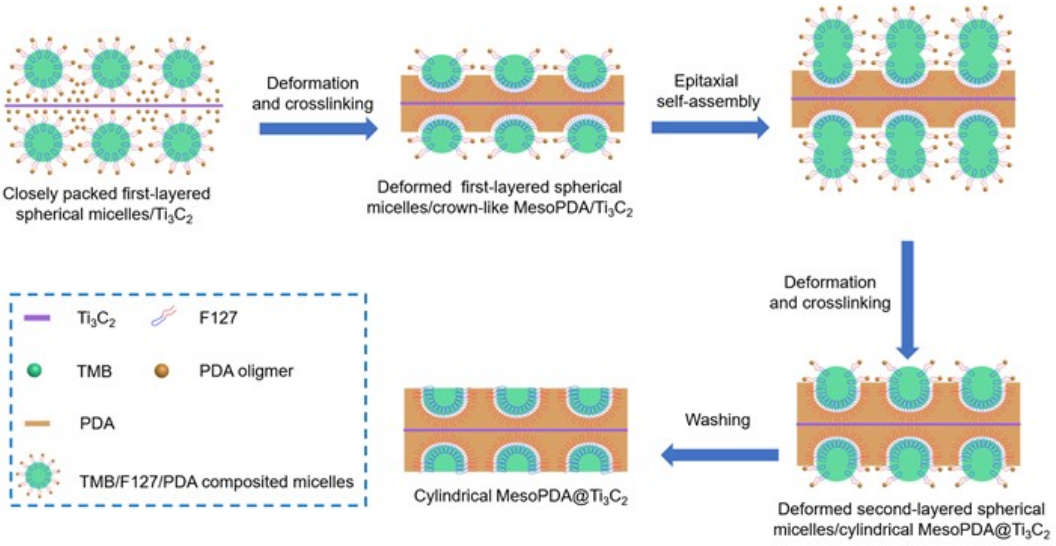

Figure S5. Schematic illustration of the formation process of highly ordered vertical mesopores by 2D model.

One epitaxial self-assembly mechanism is proposed for the synthesis of vertical mesopores in 2D MesoPDA@Ti_3C_2 heterostructure. At the initial stage, DA is firstly polymerized to form PDA oligomers, which are adsorbed on the surface of Ti_3C_2 MXene nanosheet and TMB swelled F127 micelles via coordination interaction and hydrogen bond. Then those TMB/F127/PDA composited micelles self-assemble on the surface of Ti_3C_2 MXene nanosheet to form close-packing structure in the presence of KCl, which ensures the formation of ordered mesopores. According to previous report (*J. Phys. Chem. B* **2003**, *107*, 13368-13375., *J. Am. Chem. Soc.* **2005**, *127*, 10794-10795.), the addition of KCl can reduce the critical micelle concentration (CMC) of F127 and the thermodynamic radius of micelles, and induce dehydration of ethylene oxide units from the hydrated PEO shell adjacent to the PPO core. These effects increase the rigidity of composite micelles and strengthen interactions between them, thereby promoting highly ordered self-assembly. In the following process, those spherical composited micelles deform to bowl-like structure to further decrease the interfacial tension, and those PDA oligomers mitigate to the surface of Ti_3C_2 MXene nanosheet and the edge of bowl-like structure to form PDA wall by crosslinking reaction. This indicates that those TMB/F127/PDA composited micelles are metastable and can deform into the lowest energy state when contacting with other interfaces. And then, when one new TMB/F127/PDA composited micelle approaches the bowl-like structure, the TMB both in composited micelle and bowl-like structure fuse together to decrease the interface energy and form crown-like TMB/F127/PDA composited micelles. Subsequently, those PDA oligomers crosslink with the pre-synthesized blow-like structure, leading to the further deformation of the crown-like TMB/F127/PDA composited micelles and the formation of vertical mesopores. Lastly, vertical mesopores with increasing depth form by repeating the above processes. In this case, the preformed bowl-like structure and vertical pore can act as the acceptable sites to capture TMB/F127/PDA composited micelles to promote the epitaxial growth-like self-

assembly. And thus, we call the formation mechanism of vertical mesopores as epitaxial self-assembly, which involves continuous contact-fusion-deformation-crosslinking of TMB/F127/PDA composited micelles.

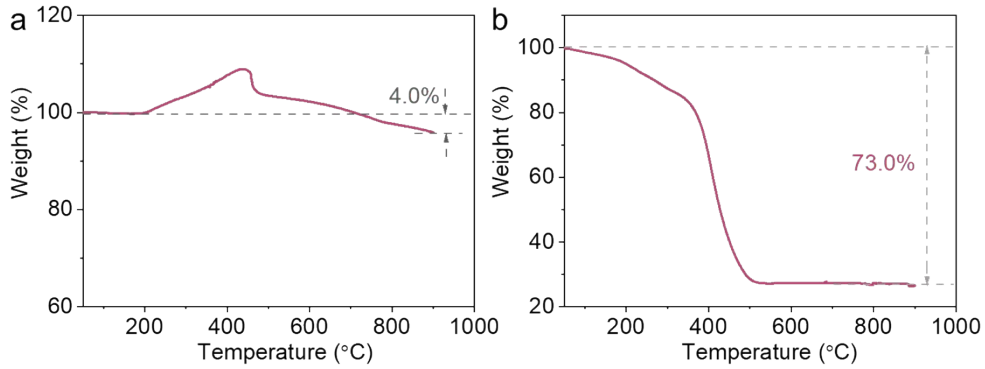

Figure S6. TGA curve of (a) Ti_3C_2 and (b) the highly ordered MesoUSC@Ti_3C_2 in air.

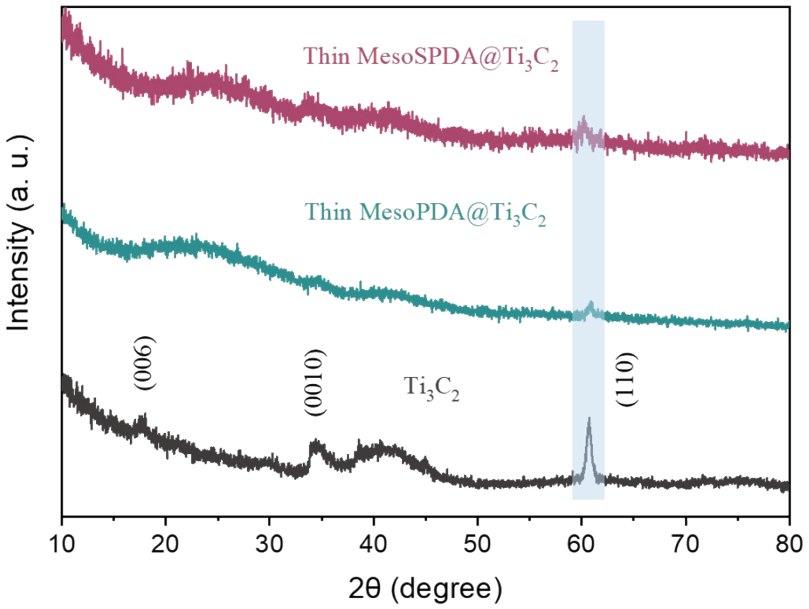

Figure S7. XRD patterns of Ti_3C_2, MesoPDA@Ti_3C_2 and MesoUSC@Ti_3C_2 with thin MesoPDA and MesoUSC layers.

To confirm the maintain of the crystalline structure after PDA coating and sulfidation treatment, we examine the XRD picture of MesoPDA@Ti_3C_2 and MesoUSC@Ti_3C_2 with thin MesoPDA and MesoUSC layers, which were fabricated by similar parameters but with 2 h reaction time. The XRD picture of Ti_3C_2 shows several typical peaks of MXene. The (004) and (0010) peaks ascribed to the stacking of the 2D nanosheets, and the (110) peak are attributed to in-plane crystalline lattice of Ti_3C_2. After coated with thin PDA and USC layers, the (004) and (0010) peaks disappeared while the (110) peak can be still observed for MesoPDA@Ti_3C_2 and MesoUSC@Ti_3C_2. This indicates that the crystalline structure of Ti_3C_2 are still maintained after PDA coating and sulfidation treatment. With thicker PDA and USC coating layers that are shown in manuscript, the (110) peak also cannot be observed. This should be due to the low content of Ti_3C_2.

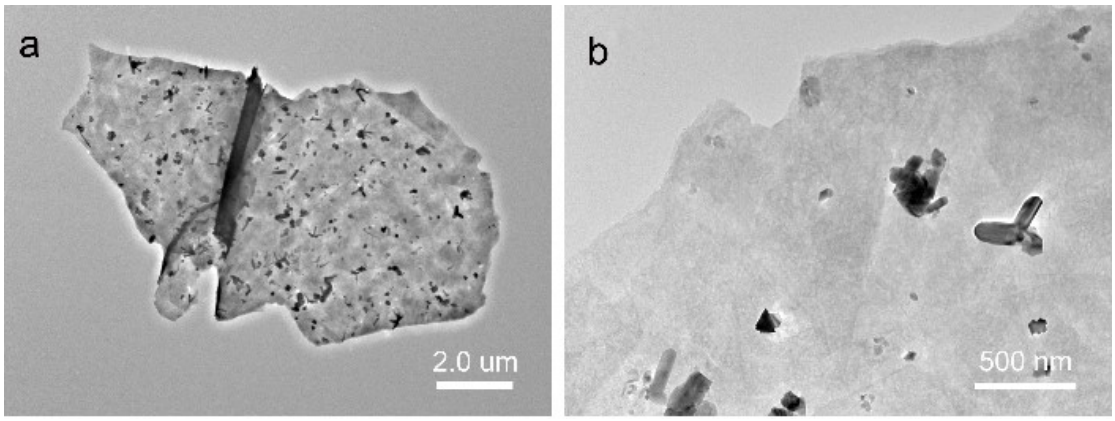

Figure S8. (a, b) TEM images of Ti_3C_2-S-600 obtained by direct sulfidation of Ti_3C_2.

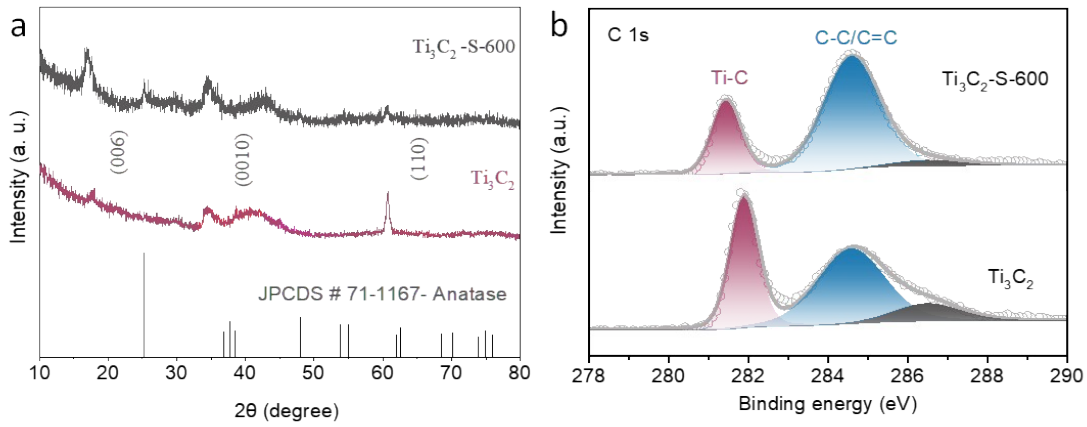

Figure S9. (c) XRD pictures and (d) C 1s XPS spectra of Ti_3C_2 and Ti_3C_2-S-600

To further confirm the stability of Ti_3C_2 during sulfidation treatment, we examine the morphology and composition of Ti_3C_2-S-600 obtained by direct sulfidation of Ti_3C_2. Even sulfidation treatment of pure Ti_3C_2 generates some nanoparticles (Figure S6a, b), and broad TiO_2 peaks (Figure S7a), the (110) peaks of Ti_3C_2 in XRD picture (Figure S7a) and Ti-C bonds of Ti_3C_2 in XPS spectra (Figure S7b) verify the retention of Ti_3C_2. Moreover, no nanoparticles are observed on TEM picture of MesoUSC@Ti_3C_2 (Figure 1c, d), indicating that PDA coating can further protect Ti_3C_2 from oxidation and ensure the maintain of its crystalline structure.

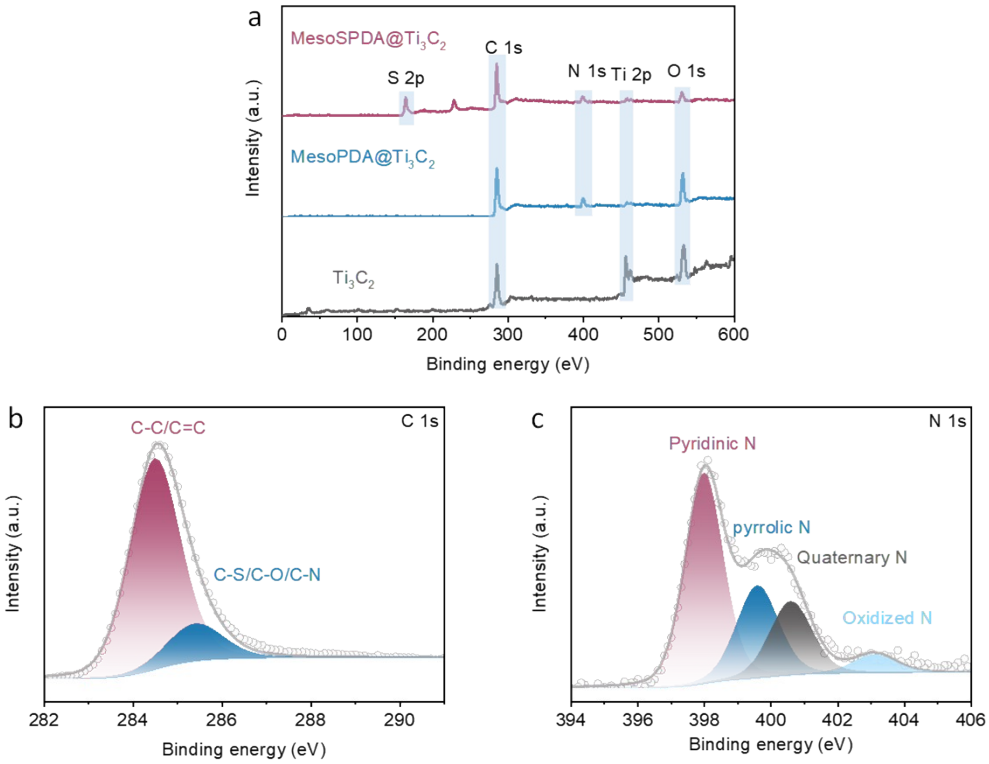

Figure S10. (a) XPS spectra of Ti_3C_2, MesoPDA@Ti_3C_2 and MesoUSC@Ti_3C_2. (b) C 1s and (c) N 1s spectra of MesoUSC@Ti_3C_2.

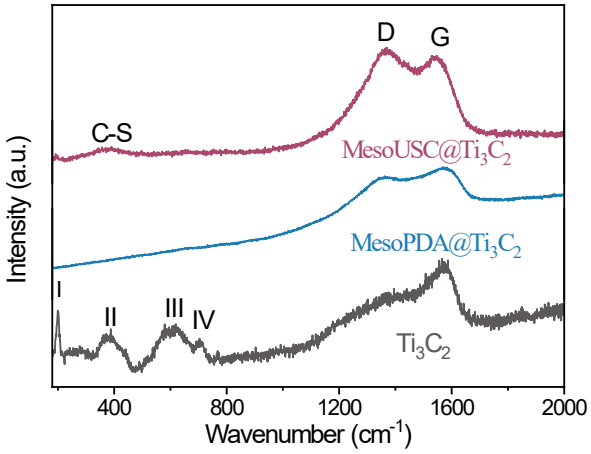

Figure S11. Raman spectra of Ti_3C_2, MesoPDA@Ti_3C_2 and MesoUSC@Ti_3C_2.

These peaks at 200 cm^{-1} and 380 cm^{-1} peaks are attributed to the out-of-plane vibrations of Ti, C and surface groups, and in-plane vibrations of surface groups, respectively. These peaks at 600 cm^{-1} and 705 cm^{-1} peaks are corresponded to the in-plane and out-of-plane vibrations of the carbon atoms.

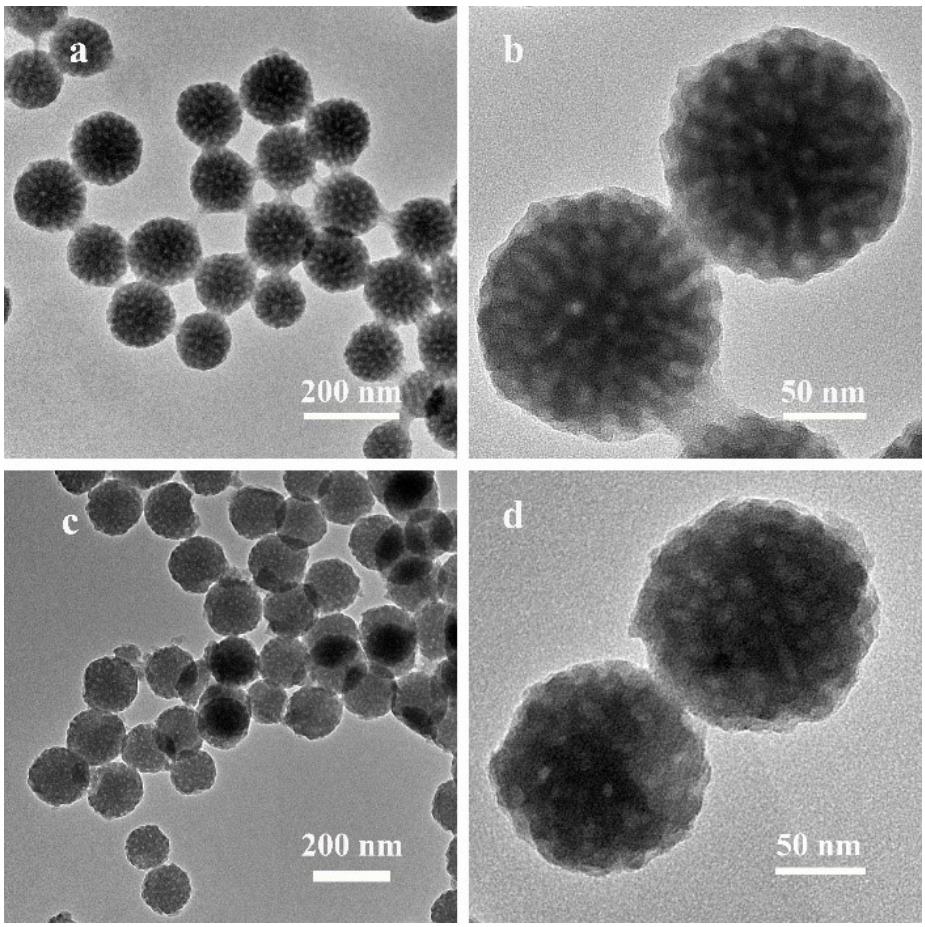

Figure S12. TEM images of (a, b) MesoPDA and (c, d) MesoUSC spheres.

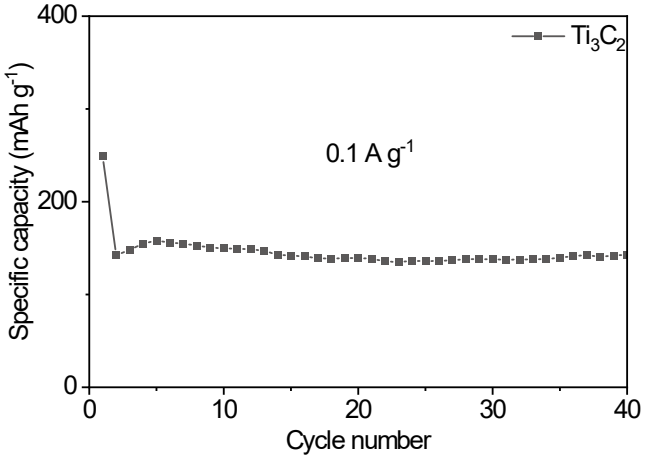

Figure S13. Cycling performances of Ti_3C_2 at 0.1 A g^{-1}.

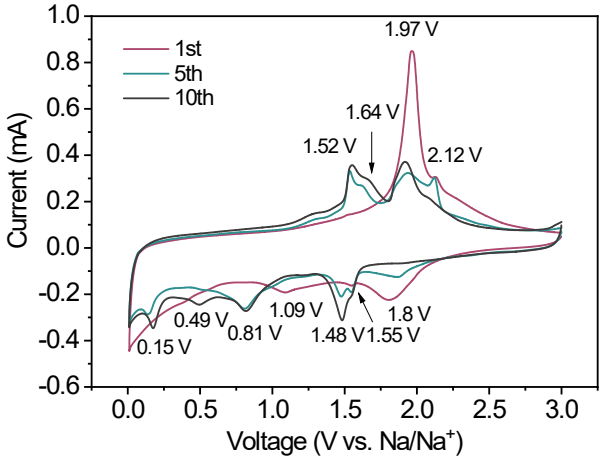

Figure S14. CV curves of MesoUSC@Ti_3C_2 at 0.1 mV s^{-1} for the first 10 cycles.

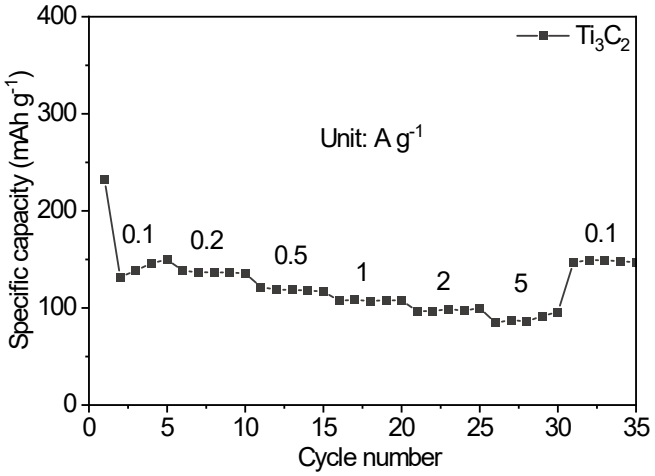

Figure S15. Rate performances of Ti_3C_2 from 0.1 to 5 A g^{-1}.

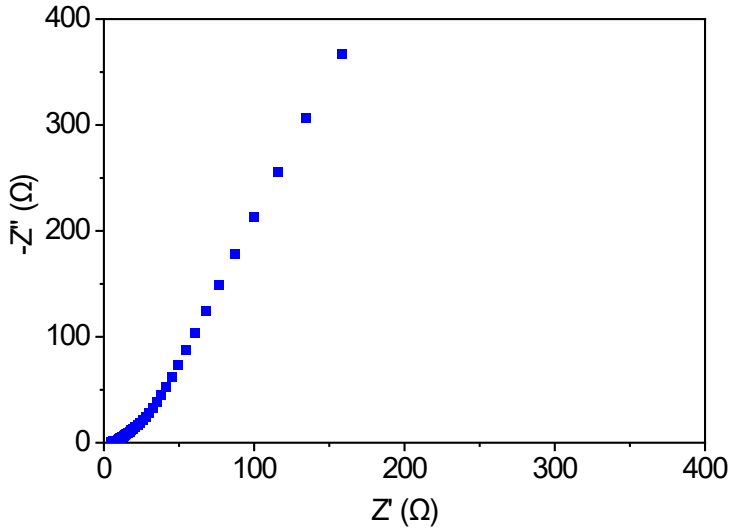

Figure S16. EIS plot of pristine Ti_3C_2 MXene.

Table S1. Elemental composition of ultrahigh level sulfur-doped carbon in MesoUSC@Ti_3C_2

Sample	C (wt%)	H (wt%)	O (wt%)	S (wt%)	N (wt%)
SPDA	47.4	2.0	18.2	26.2	6.2

Table S2. Comparison of the rate performances of MesoUSC@Ti_3C_2 for sodium storage with sulfur-doped carbon-based materials, and other MXene-based composites reported in the literatures.

Sulfur content of sample	Capacity at different current density, A g^{-1}/ mAh g^{-1}					Ref.
26.2 wt % in USC	0.2/513	0.5/515	1/511	2/500	5/463	This work
7.28 wt %	0.2/426	1/307	2/276	10/236	NA	[2]
23.79 wt %	0.2/293	0.5/245	1/207	2/152	3/110	[3]
26.9 wt %	0.2/320	0.4/302	1/275	2/211	4/158	[4]
9.19 wt %	0.2/280	0.5/250	1/220	2/190	5/150	[5]
12.46 at%	0.2/483	0.5/436	1/390	2/257	NA	[6]
21.5 wt%	0.2/445.4	0.4/418.1	0.8/387.5	1.6/346.7	3.2/283.7	[7]
49.54 wt%	0.2/444.7	0.5/401.9	1/361.9	2/294.6	NA	[8]
8.2 at%	0.2/482.8	0.5/447.0	1/391.6	2/346.1	5/306.7	[9]
18 wt%	0.2/335.88	0.4/257.94	0.8/187.92	1/117.9	2/94.86	[10]

References:

[1] F. Bu, Z. Sun, W. Zhou, Y. Zhang, Y. Chen, B. Ma, X. Liu, P. Liang, C. Zhong, R. Zhao, H. Li, L. Wang, T. Zhang, B. Wang, Z. Zhao, J. Zhang, W. Li, Y. S. Ibrahim, Y. Hassan, A. Elzatahry, D. Chao, D. Zhao, *J. Am. Chem. Soc.* **2023**, *145*, 24284-24293.

[2] W. Song, J. Kan, H. Wang, X. Zhao, Y. Zheng, H. Zhang, L. Tao, M. Huang, W. Liu, J. Shi, *ACS Appl. Nano Mater.* **2019**, *2*, 5643-5654.

[3] J. Yan, W. Li, P. Feng, R. Wang, M. Jiang, J. Han, S. Cao, K. Wang, K. Jiang, *J. Mater. Chem. A* **2020**, *8*, 422-432.

[4] W. Li, M. Zhou, H. Li, K. Wang, S. Cheng, K. Jiang, *Energy Environ. Sci.* **2015**, *8*, 2916-2921.

[5] J. Yang, X. Zhou, D. Wu, X. Zhao, Z. Zhou, *Adv. Mater.* **2017**, *29*, 1604108.

[6] X. Yuan, S. Chen, J. Li, J. Xie, G. Yan, B. Liu, X. Li, R. Li, L. Pan, W. Mai, *Carbon Energy* **2021**, *3*, 615-626.

[7] K. Chen, H. Li, Y. Xu, K. Liu, H. Li, X. Xu, X. Qiu, M. Liu, *Nanoscale* **2019**, *11*, 5967-5973.

[8] L. Zhang, W. Zhang, Z. Zhu, Q. Huang, X. Liu, M. Zhang, W.-B. Pei, J. Wu, *J. Solid State Chem.* **2021**, *301*, 122359.

[9] X. Luo, L. Ma, Z. Li, X. Zhao, Y. Dong, Q. Yang, H. Liu, B. Wang, L. Zhi, Z. Xiao, *J. Mater. Chem. A* **2021**, *9*, 24460-24471.

[10] L. Fan, R. Ma, Y. Yang, S. Chen, B. Lu, *Nano Energy* **2016**, *28*, 304-310.